Geophysical Journal International

Geophys. J. Int. (2016) **205,** 1843–1858
Advance Access publication 2016 April 3
GJI Gravity, geodesy and tides

doi: 10.1093/gji/ggw122

Constraints on seasonal load variations and regional rigidity from continuous GPS measurements in Iceland, 1997–2014

Vincent Drouin,[1] Kosuke Heki,[2] Freysteinn Sigmundsson,[1] Sigrún Hreinsdóttir[3] and Benedikt G. Ófeigsson[4]

[1] *Nordic Volcanological Center, Institute of Earth Sciences, University of Iceland, Sturlugata* 7, IS-101 *Reykjavík, Iceland. E-mail: vjp1@hi.is*
[2] *Department of Earth and Planetary Sciences, Hokkaido University, Sapporo* 060-0810, *Japan*
[3] *GNS Science, Lower Hutt* 5040, *New Zealand*
[4] *Icelandic Meteorological Office,* IS-101 *Reykjavík, Iceland*

Accepted 2016 March 30. Received 2016 March 30; in original form 2016 January 21

SUMMARY

Two types of signals are clearly visible in continuous GPS (cGPS) time-series in Iceland, in particular in the vertical component. The first one is a yearly seasonal cycle, usually sinusoid-like with a minimum in the spring and a maximum in the fall. The second one is a trend of uplift, with higher values the closer the cGPS stations are to the centre of Iceland and ice caps. Here, we study the seasonal cycle signal by deriving its average at 71 GPS sites in Iceland. We estimate the annual and semi-annual components of the cycle in their horizontal and vertical components using a least-squares adjustment. The peak-to-peak amplitude of the cycle of the vertical component at the studied sites ranges from 4 mm near the coastline up to 27 mm at the centre of the Vatnajökull, the largest ice cap in Iceland. The minimum of the seasonal cycle occurs earlier in low lying areas than in the central part of Iceland, consistent with snow load having a large influence on seasonal deformation. Modelling shows that the seasonal cycle is well explained by accounting for elastically induced surface displacements due to snow, atmosphere, reservoir lake and ocean variations. Model displacement fields are derived considering surface loads on a multilayered isotropic spherical Earth. Through forward and inverse modelling, we were able to reproduce *a priori* information on the average seasonal cycle of known loads (atmosphere, snow in non-glaciated areas and lake reservoir) and get an estimation of other loads (glacier mass balance and ocean). The seasonal glacier mass balance cycle in glaciated areas and snow load in non-glaciated areas are the main contributions to the seasonal deformation. For these loads, induced seasonal vertical displacements range from a few millimetres far from the loads in Iceland, to more than 20 mm at their centres. Lake reservoir load also has to be taken into account on local scale as it can generate up to 20 mm of vertical deformation. Atmosphere load and ocean load are observable and generate vertical displacements in the order of a few millimetres. Inversion results also shows that the Iceland crust is less rigid than the world average. Interannual deviation from the GPS seasonal cycle can occur and are caused by unusual weather conditions over extended period of time.

Key words: Time-series analysis; Inverse theory; Satellite geodesy; Kinematics of crustal and mantle deformation; Rheology: crust and lithosphere; Atlantic Ocean.

1 INTRODUCTION

A network of more than 100 continuously recording GPS stations (cGPS) is currently operated in Iceland. The two IGS (International GNSS Service) stations, REYK and HOFN, are the longest running continuous sites, established in 1995 and 1997, respectively. In 1999, six additional sites were added and between 2000 and 2005 the network continued to grow with 16 additional stations. A fast expansion occurred between 2006 and 2009 with 40 new site installations (Geirsson *et al.* 2010). The daily operation of many of the sites is overseen by the Icelandic Meteorological Office (IMO) and the National Land Survey of Iceland. Important contributing institutions to the network include University of Arizona, USA; University of Savoie, France; Pennsylvania State University, USA;

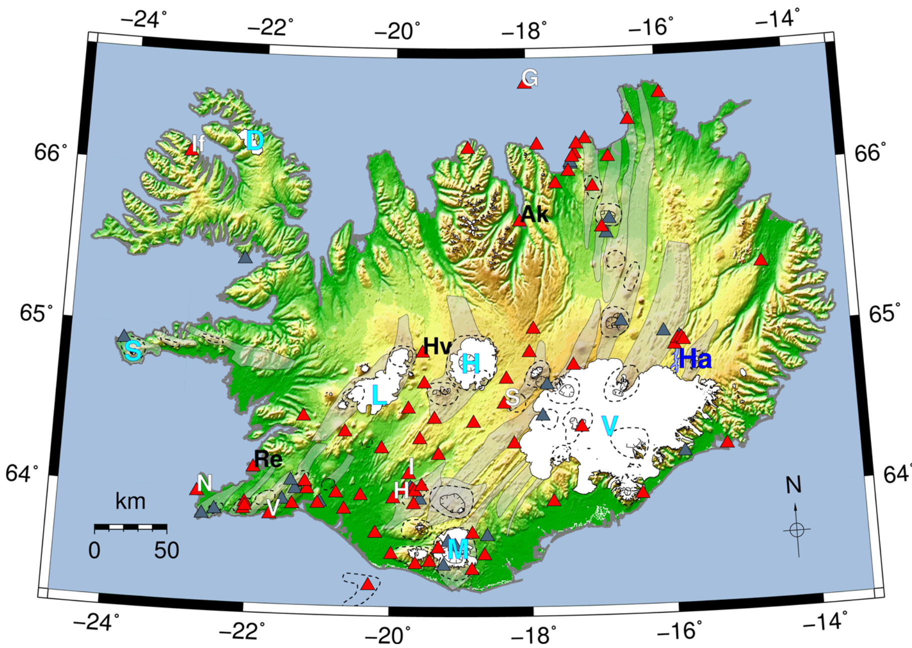

Figure 1. Location of cGPS stations in Iceland installed prior to 2014 August. Red triangles show stations used in this study and dark grey triangles stations that were not used. Background shows topography and ice caps (white areas). Fissure swarms (transparent grey areas), outline of central volcanoes (dashed lines) and calderas (comb lines) are after Jóhannesson & Sæmundsson (2009). Name of glaciers are indicated in cyan (D: Drangajökull, S: Snæfelsjökull, L: Langjökull, M: Mýrdalsjökull, H: Hofsjökull, V: Vatnajökull). Hálslón reservoir is indicated by the blue area next to the blue letters (Ha). Name of selected GPS sites mentioned in the text are indicated in white (If: ISAF, N: NYLA, V: VOGS, H: HAUD, I: ISAK, S: SKRO, G: GMEY). IMO weather stations mentioned in text are indicated in black (Re: Reykjavík, Hv: Hveravellir, Ak: Akureyri).

ETH Zurich, Switzerland; King Abdullah University of Science and Technology, Saudi Arabia and Bavarian Academy of Sciences and Humanities, Germany.

The cGPS network in Iceland records the plate spreading in Iceland (Geirsson *et al.* 2006), as well as an uplift signal that has been extensively studied with various techniques and is related to glacial isostatic adjustment due to present-day glacial retreat (Árnadóttir *et al.* 2009; Auriac *et al.* 2013). There is evidence that the uplift rates due to present-day glacial retreat are accelerating with time (Compton *et al.* 2015a). The discrimination between load-variation-induced deformation and magma-induced deformation is important in Iceland for hazard assessment (e.g. Pinel *et al.* 2007). The topic of this paper is the average seasonal cycle, a term we use to refer to a cycle that repeats on a yearly basis. We model it as composed of an annual component with a one year period and a semi-annual component with a half a year period. The seasonal cycle signal in Iceland has been studied, considering winter and summer glacier mass balance by Grapenthin *et al.* (2006). They considered the seasonal cycle of 18 cGPS stations with long enough time-series at the time of that study. The cycle was interpreted in terms of annual load variations at the Icelandic ice caps on a half-space Earth model with uniform elastic parameters. Here, we use 71 cGPS time-series of daily positions (Fig. 1). The longest time-series is 17 yr, from the REYK station in Reykjavík. We model the Earth response due to load changes using a spherical Earth model, instead of a simple elastic half-space, and we consider various surface loads, similarly to Heki (2004). Snow remains the most important load but there is evidence for induced surface displacements due to variations in atmosphere, ocean and lake reservoir loads as well.

Snow accumulation during winter is known to generate vertical displacements up to centimetre scale (Heki 2001). Grapenthin *et al.* (2006) showed that glacier mass balance can account for a large part of the seasonal cycle observed in GPS in Iceland. Glaciers are gaining mass during the winter and spring with snow accumulation and losing mass during summer and fall with melting. In addition, glaciers in Iceland had a negative yearly mass balance from 1995 to 1996 (Björnsson *et al.* 2013) until 2014–2015, when the mass balance became positive again (Finnur Pálson, private communication, 2015). This is a secular trend and thus does not affect the seasonal cycle estimation.

Atmospheric pressure loading is known to be able to displace the Earth's surface over a centimetre on subdiurnal timescales (van Dam *et al.* 1994). GPS solutions over a 24 hr period are sufficient to average out this deformation (Tregoning & van Dam 2005), even though correcting for subdaily atmospheric pressure variations at tidal frequencies would improve the observations results (Tregoning & Watson 2009). Here, we used daily solutions for our GPS time-series so we are not expecting to see any effect of such short atmospheric pressure change. However, we expect a contribution from a seasonal atmospheric pressure variation in Iceland.

Ocean tidal loading is known to generate important displacements at coastal GPS stations on a subdaily and weekly basis. We corrected for these during the data analysis by using the FES2004 model, a mesh of global hydrodynamic tide solutions (Lyard *et al.* 2006). However, this model does not account for semi-annual, annual and longer cycles in the tides, nor for non-tidal ocean variation.

Variable mass of water in lakes provides load changes on the surface of the Earth. A large cycle occurs at some reservoirs for hydropower stations; they fill up in summer and then lower in the winter time. Such reservoirs can have an important effect in their surrounding areas. Hálslón reservoir is the largest reservoir in Iceland with an area of approximately 56 km^2 and a water volume of 2.1 km^3 when full. cGPS stations were installed for monitoring purpose when it was constructed and first filled in 2006. Their data are of importance for our study as they are the only cGPS north-east of the Vatnajökull ice cap. The seasonal load variation induced by changes in the level of this reservoir show up clearly in the observations.

In the following, we begin with the calculation and analysis of the seasonal cycle of the east, north and up displacement time-series of the cGPS sites. We also present *a priori* information on the seasonal cycle within data sets on snow accumulation in non-glaciated areas, atmospheric pressure and variation of the Hálslón reservoir level. Additional information about the seasonal load variation and the elastic properties of the Earth are then derived from the inversion of the cGPS seasonal cycles. The amount of deformation that each of the load generates is then computed using a best-fitting Earth model.

2 DATA

2.1 GPS

Daily GPS solutions were calculated at University of Iceland with the GAMIT/GLOBK 10.4 GPS analysis software, in the ITRF2008 reference frame using over 100 worldwide reference stations. Only GPS satellites with a good phase centre location were included in the processing to prevent any scale error in the GPS solutions (Zhu *et al.* 2003). The data were corrected for ocean tidal loading using the FES2004 model (Lyard *et al.* 2006). Most of the GPS data used in this study are available as RINEX files at the FUTUREVOLC data hub (see Acknowledgments). Here, we study the time period prior to a rifting episode in the Bárðarbunga volcanic system that began in 2014 August and was associated with large-scale deformation (Sigmundsson *et al.* 2014). We visually checked each of the time-series and excluded the ones with less than two full years of data or those with data gaps over extended periods of time each year. We kept 71 stations after this check.

The east, north and up displacement components of each station were analysed separately for evaluation of seasonal cycle. The entire time-series were used to determine the annual and semi-annual components of the deformation. We first filtered out all daily solutions that had a standard deviation of more than 5 mm for the horizontal or more than 10 mm for the vertical. The amplitude of the seasonal displacements appears to be relatively constant from year to year. A temporally varying amplitude approach like the one used by Bennett (2008) is thus not necessary. Trends in time-series were then estimated using a software developed and used in previous studies of the seasonal cycle (Heki 2001, 2004). Using least squares, it calculates the best fit for secular (linear or polynomial), annual (sinusoidal) and semi-annual (sinusoidal) components. The displacement D of a GPS station as a function of time t (in decimal years) can then be written in the form of a linear equation:

$$D(t) = a + b \cdot t + c \sin(2\pi t) + d \cos(2\pi t) + e \sin(4\pi t) + f \cos(4\pi t) \quad (1)$$

In this case, linear (a and b), annual (c and d) and semi-annual (e and f) components are taken into account. Additional terms m_p for fitting a polynomial of degree n instead of a line can be added to eq. (1) as follows: $\sum_{p=2}^{n} m_p \cdot t^p$. The software also allows for correction of jumps, changes of trend and exponential transient movements. This allowed us to remove time-series irregularities due to antenna change and earthquakes in south Iceland in 2000 and 2008 that were clearly visible on stations close to the earthquake epicentres (e.g. Hreinsdóttir *et al.* 2009; Decriem *et al.* 2010). Deformation signals of volcanic origin occurring over extended period of time,

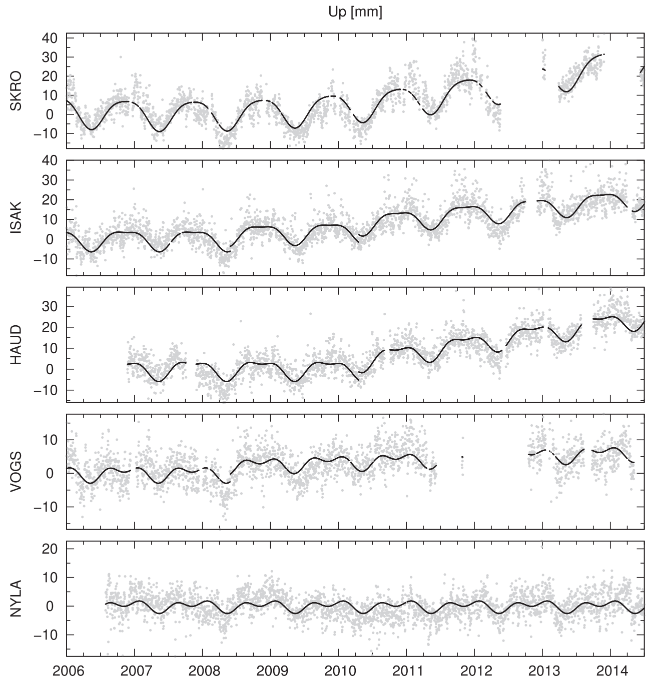

Figure 2. Up component time-series at selected GPS sites. Grey dot shows observed data (daily estimates of the vertical component), black line shows a best-fitting curve considering linear, semi-annual and annual components as in eq. (1). The curve for station SKRO also includes a second-order polynomial to account for the acceleration of uplift related to ice cap retreat. Initial linear trend is removed from each time-series. Jumps and/or change of trend are visible in 2010 for ISAK and HAUD because of the Eyjafjallajökull eruption and in 2008 for VOGS and ISAK because of the M6.2 south Iceland earthquakes. Location of each station is shown on Fig. 1.

like the one prior to and associated with the Eyjafjallajökull eruption in 2010 (Sigmundsson *et al.* 2010), are not easy to correct for. Therefore, the data influenced by such signals were removed from the time-series. In these cases, we allowed a jump and/or a change in trend in the data gaps created. All other small non-periodic deviations are minimized during the trend estimation and were thus considered to not affect significantly the annual and semi-annual cycles estimation. Examples of up component time-series are shown in Fig. 2.

Results show that, in the vertical component, all cGPS stations have a seasonal local minimum in the spring, most of them in May around day 130–140 of the year (Fig. 3). This is similar to day 140 found by Grapenthin *et al.* (2006). Seasonal cycles in the vertical component show that the GPS stations are relatively stable between September and January, subside from January until May and then rise from May until September. There is also a systematic pattern such that the further the stations are from central Iceland, the earlier they have their minimum. A similar gradient is observed for the signal amplitude. Stations in central Iceland have the highest amplitudes especially the ones near Vatnajökull, the largest ice cap in Iceland, while the ones near the coast have the smallest amplitude.

The above-mentioned systematics are an indication that the snow and ice load variations are a dominant factor influencing the seasonal cycle observed by the cGPS network. The spatial distribution of the signal and its minimum in May correlates with snow accumulation. The timing of the yearly minimum in the vertical component can be attributed to the snow starting to melt earlier in low lying areas near the coastline areas compared to

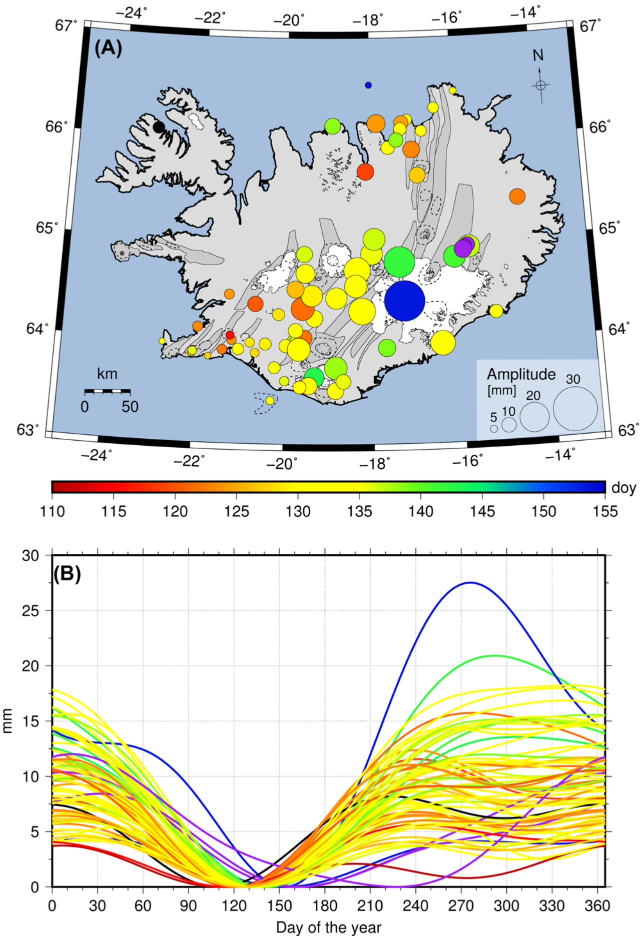

Figure 3. Seasonal cycle of GPS vertical component. (A) Time of minimum and amplitude of the estimated seasonal cycle of the cGPS vertical components. Circles show cGPS stations: size shows the amplitude of the seasonal signal and colour shows the day of the year of the minimum (black means earlier than day of year (doy) 110 and purple means later than doy 155). (B) Seasonal cycle for each cGPS with the same colour scale as in A. Each seasonal cycle is shown relative to its minimum.

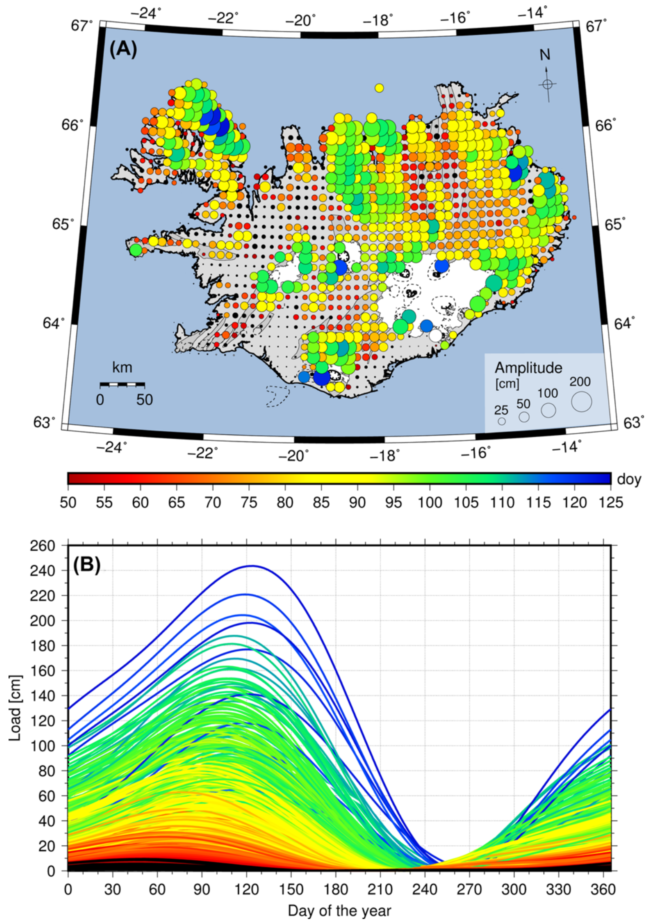

Figure 4. Seasonal cycle of snow load in centimetres of water equivalent derived from a data set provided by the Icelandic Meteorological Office. (A) Time of minimum and amplitude of the estimated seasonal cycle of the snow load. Circles show data points: size shows the amplitude of the seasonal signal and colour shows the day of the year of the minimum (black means earlier than doy 50 and white means later than doy 125). (B) Seasonal cycle for each location shown in (A) with the same colour scale. Each seasonal cycle is shown relative to its minimum. The data were resampled at 0.2° longitude and 0.1° latitude to make the plot clearer.

the central part of Iceland. A few stations deviate from that pattern, like GMEY, located on the Grímsey island and ISAF in the Westfjords (Fig. 1).

2.2 Snow

The IMO provided snow water equivalent (SWE) load estimation over non-glaciated areas of Iceland over the period from 2009 October until 2014 July (Nikolai Nawri, IMO, private communication, 2015). They calculated the snow accumulation using the Harmonie non-hydrostatic meteorological model (Seity *et al.* 2011) to dynamically downscale the ERA-Interim reanalysis, a global data set of atmospheric parameters from 1979 and continuously updated in real time (Dee *et al.* 2011), and validated the results with precipitation measurements at gauges. The data were provided as snow load values in a grid of 2.5 km by 2.5 km pixels. Glacier areas are not included in this data set because seasonal crustal loading on the glaciers is also affected by ablation of glacier ice and redistribution of the ice with the glacier flow. We estimated the snow accumulation seasonal cycle for non-glaciated areas in Iceland using the same program as for the GPS data. Beforehand, the data were resampled to a grid of 0.06° longitude by 0.03° latitude pixels to keep the computational time reasonable. The average standard deviation is about 7.4 cm of water equivalent. Results show that snow load seasonal cycles have a maximum in April and a minimum in September for most of Iceland (Fig. 4). There is a correlation between the signal amplitude and the timing of its maximum and minimum. The central part of Iceland has more snow accumulation and the maximum there occurs later than in low lying areas near the coast. This is consistent with the phase lag between the coastal cGPS and the highland cGPS being caused by snow melting earlier in low lying areas than at higher elevations.

2.3 Atmospheric pressure

We used the ERA-Interim data set (Dee *et al.* 2011) to estimate seasonal pressure variation. On the ECMWF (European Centre for Medium-Range Weather Forecasts) website, we requested daily sea level pressure measurements from the start of 1995 until the end of 2014 (see the link shown in Acknowledgments). The data were provided as atmospheric pressure in pixels of 0.75° longitude by 0.75° latitude. The ERA-Interim pressure data were compared to

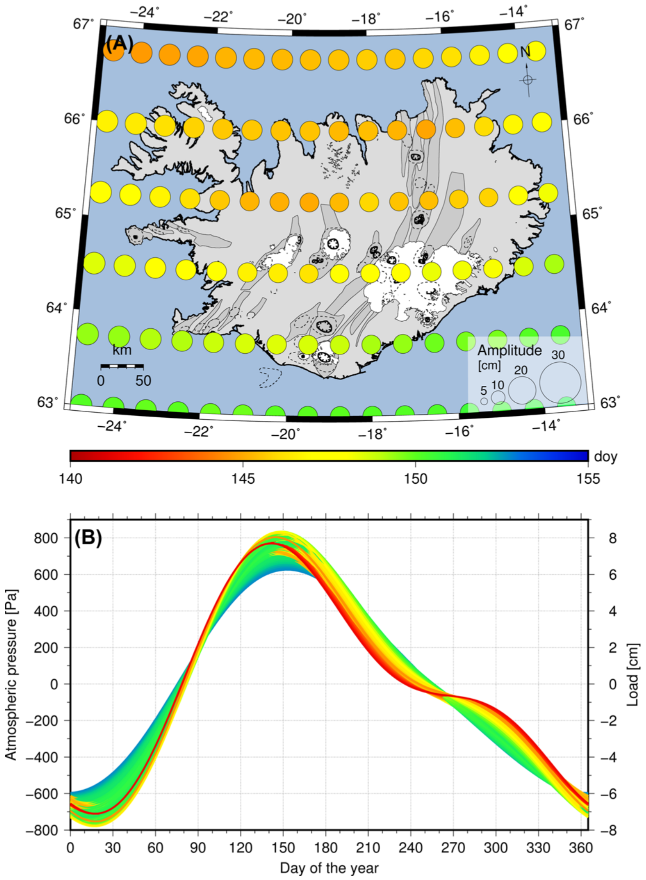

Figure 5. Seasonal cycle of sea level atmospheric pressure derived from the ERA-Interim data set. (A) Time of minimum and amplitude of the estimated seasonal cycle of the atmospheric pressure. Circles show data points: colour shows the day of the year of the minimum and size shows the amplitude of the seasonal signal. (B) Seasonal cycle for each location show in (A) with the same colour scale. Each seasonal cycle is centred on 0.

measurements at three weather stations in Iceland: Reykjavík, Akureyri and Hveravellir (Tómas Jóhannesson, IMO, private communication, 2015—Fig. 1). We found that the two data set were in good agreement with each other. We then extracted the annual and semi-annual components of sea level pressure over Iceland using the same program as for GPS. We got a fairly homogeneous signal over Iceland with an average amplitude of about 16 hPa, a minimum in January and a maximum in June (Fig. 5). The average standard deviation after trend estimation was about 13.5 hPa. This can be explained by the occurrence of rapid pressure variations up to 80 hPa on a weekly scale. The atmospheric pressure can be expressed in water equivalent as 1 hPa equals pressure from a 10 mm thick layer of water. Atmospheric load applies only on land and not on sea floor as the ocean surface height compensates automatically any atmospheric pressure change. However, the atmospheric pressure data originally come in square pixels of 0.75° of latitude/longitude and is thus covering area of sea around Iceland. Thus, in order to improve further atmospheric loading calculation, the data were resampled in pixels of 0.2° of longitude and 0.1° of latitude. The load in pixels fully over sea areas was set to zero. This minimizes applied load over water (with pixels overlapping with the coast line), while allowing a reasonable computing performance.

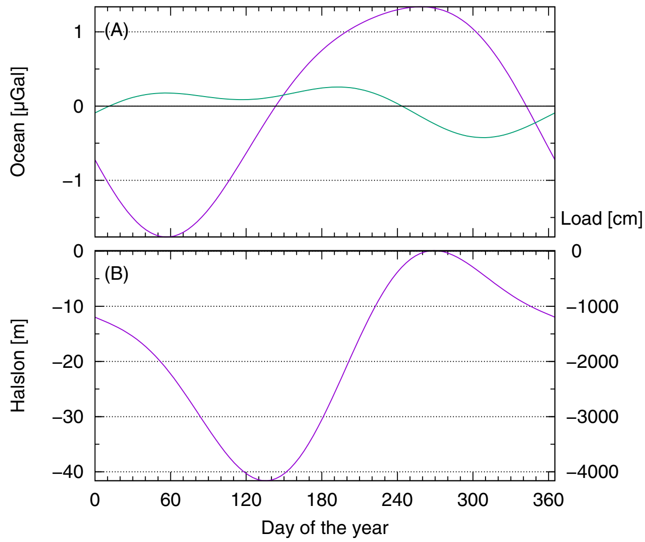

Figure 6. Seasonal cycles of ocean gravity date and the Hálslón reservoir. (A) Gravity in the Arctic ocean (purple line) and the Atlantic ocean (green line) at selected coordinates (see the text). (B) Lake level of Hálslón reservoir.

2.4 Ocean

The FES2004 ocean loading model used during the processing of the cGPS data does not include semi-annual or annual tide components. Therefore, there is a need to consider if such variations can have an influence on the derived time-series. For this, we did not use tide gauge measurements as such observations cannot be directly related to ocean load variations as temperature and salinity of the water have to be taken into account. In order to get an overview of a possible seasonal cycle in the ocean loading we used monthly GRACE satellite gravity solutions (Level-2 data, Release 5) by the Center for Space Research, University of Texas, from 2004 to 2014. We applied the anisotropic fan filter with averaging radius of 300 km to reduce short wavelength noise (Zhang *et al.* 2009) together with the decorrelation filter using polynomials of degree 3 for coefficients with orders 15 or higher to alleviate longitudinal stripes (Swenson & Wahr 2006). No hydrological model was used. This approach is similar to the one use by Heki & Matsuo (2010). We estimated the annual and semi-annual cycle of the gravity at two location near Iceland: one in the Arctic Ocean (70°N, 10°W) and another in the Atlantic ocean (62°N, 20°W). The standard deviation was about 1.3 µGal. The location in the Arctic ocean has a fairly important seasonal cycle of about 3 μGal with a minimum around March and a maximum in the fall (Fig. 6). For the area studied in the Atlantic, there was no clear seasonal cycle. We converted this gravity data into water thickness equivalent using equations given by Wahr *et al.* (1998).

2.5 Hálslón reservoir

Lake-level measurements of the Hálslón reservoir at the Kárahnjúkar power plant 2006–2015 were provided by Landsvirkjun, the Icelandic National Power company. The seasonal cycle was estimated in the same way as for the other data sets. On average, the lake-level change is about 40 m per year with a standard deviation of about 6.4 m after trend estimation from eq. (1) (Fig. 6). The reservoir normally fills up from mid-May to the end of September and then drains during the rest of the year.

Table 1. Earth models and Green's functions used in this study to get Hálslón load amplitude, while inverting for seven loads (Vatnajökull, Mýrdalsjökull, Langjökull and Hofsjökull, snow on non-glaciated areas, atmosphere, ocean and Hálslón). Maximum of the GPS up component Weighted root mean squares (WRMS) is indicated.

Model	Rheology	Green's functions	Hálslón	$WRMS_{max}$(U)
Gutenberg–Bullen	Alterman *et al.* (1961)	Farrell (1972)	45.4 ± 2.5 m	1.70 mm
G-B continental	Harkrider (1970)	Farrell (1972)[a]	42.8 ± 2.4 m	1.71 mm
1066A	Gilbert & Dziewonski (1975)	Okubo & Saito (1983)	24.7 ± 1.5 m	1.84 mm
PREM	Dziewonski & Anderson (1981)	Guo *et al.* (2004)[b]	38.9 ± 2.2 m	1.73 mm

[a]For depth greater than 1000 km the Gutenberg–Bullen rheology is used.
[b]The ocean and upper crust from the PREM are mixed in one single homogeneous layer.

3 MODELLING

3.1 Setup

For load variations occurring on a short timescale, we expect the upper part of the Earth to behave elastically. Considering the dimensions of Iceland (approximately 300 km by 200 km), we used elastic and isotropic spherical Earth models for modelling of ground displacements induced by surface loading. In order to calculate such displacements, these models are represented as a Green's functions table (as e.g. described by Farrell (1972) and Guo *et al.* (2004)). The models have radially varying elastic properties. The following models and associated Green's tables were considered: the PREM, the Gutenberg–Bullen model, the G-B continental shield model and the 1066a model (see Table 1 and Fig. 7). For the PREM model, Guo *et al.* (2004) mixed the ocean layer and uppermost crustal layer in a single homogeneous layer with elastic moduli being equal to those of the original crustal layer.

We used an inversion process to constrain the surface loading and check the quality of the employed models. We utilized a program that links displacements and loads through spherical Earth Green's functions as described above (Heki 2004). For a given day, it finds the best-fitting load over a set of given areas by minimizing the seasonal GPS cycles residuals with least-squares adjustments. We derived seasonal cycle for the inferred loads through inversion of the GPS displacements sampled every 5 day of a year from day 1 to 361 (a total of 72 separate inversions for deriving a yearly cycle). All cGPS seasonal cycles were set relative to day 270 of the year for the inversion (September 26–27). It was chosen for reference because it is within the stable part of the seasonal cycle for most of the cGPS stations; about three months before main snow accumulation begins in January and after the melting of the previous winter snow.

Surface loads that were inverted for were defined as grids of square pixels, with each pixel given a load scale factor (the default value of 1 gives loads directly in centimetres of water equivalent). Here, we considered atmosphere, ocean, the Hálslón reservoir, glaciers and snow on non-glaciated areas (Fig . 8). To explain the observed seasonal cycle, we tried several combination of loads in these areas. The resulting best-fitting model solves for loads in three areas: (i) glaciers, as one area with predefined load scale factor between glaciers, (ii) atmosphere and (iii) ocean. Effects of snow in non-glaciated areas are considered by removing its effect prior to the inversion.

Iceland as a whole was considered as the area of uniform atmospheric loading. Ocean was represented by a 200 km buffer area outside the coast of Iceland. Hálslón reservoir was represented by the area it covers when the lake level is at its maximum. Glaciers were divided into three distinct sets: (i) Vatnajökull, (ii) Mýrdalsjökull and Eyjafjallajökull and (iii) Langjökull and Hofsjökull (Fig. 1). Snæfellsjökull and Drangajökull were ignored because of their small size and the limited cGPS in their surroundings. Mýrdalsjökull and

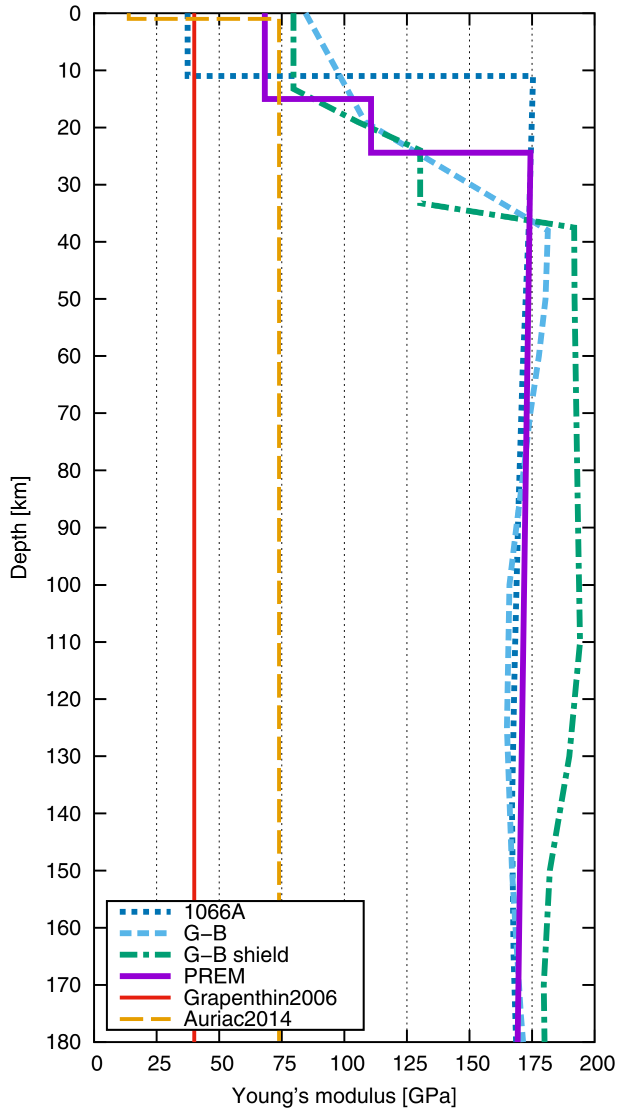

Figure 7. Young's modulus of the upper part of four global Earth models (1066A, Gutenberg–Bullen, Gutenberg–Bullen continental shield and PREM) and two best-fitting models for Iceland from earlier studies (Grapenthin *et al.* 2006; Auriac *et al.* 2014).

Eyjafjallajökull were merged into a single area as we expected them to behave in a similar way. Langjökull and Hofsjökull area were also merged into a single area because of the unrealistic inversion results obtained when they were separate loads. In this merged area, the two glaciers were given a relative load scale factor (1 for Hofsjökull and 1.32 for Langjökull) proportional to the ratio between their expected relative mass balance given by Finnur Pálsson (private

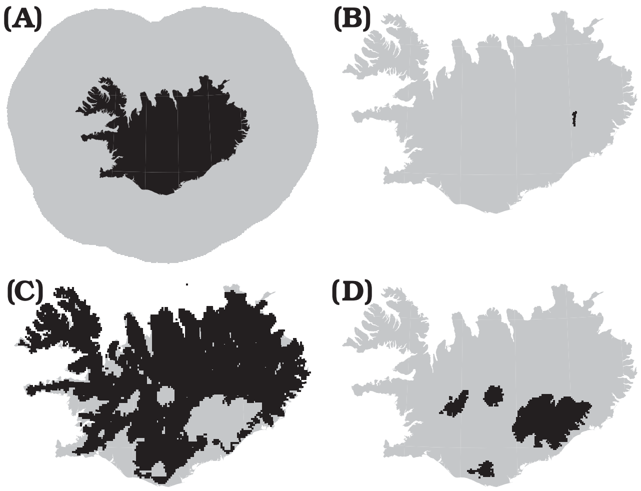

Figure 8. Areas covered by each of the inverted loads. (A) Ocean (grey), atmosphere (black). (B) Hálslón (black). (C) Snow in non-glaciated areas (black). (D) Glaciers (black). See Fig. 1 for names of glaciers.

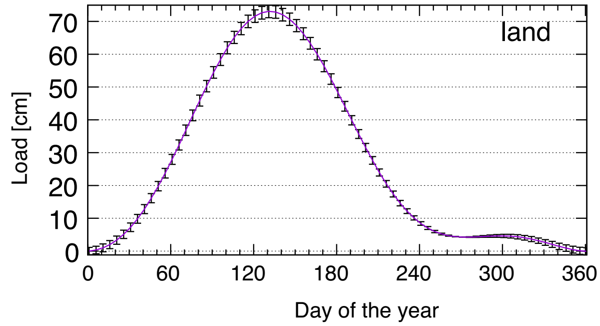

Figure 9. Seasonal cycle for a uniform load over Iceland obtained from inverting the cGPS vertical seasonal cycles using the unscaled PREM model. Load is given in centimetres of water equivalent. Seasonal cycle is shown relative to January 1. Error bars show $1-\sigma$ standard deviation.

communication, 2015) and Grapenthin *et al.* (2006). The three glaciers sets were also merged into one load and given a relative load scale factor to form additional sets for inversion. Giving Vatnajökull a load scale factor of 1, we used relative load scale factors of 1.126, 0.833 and 1.667 for Langjökull, Hofsjökull and Mýrdalsjökull respectively. Snow on non-glaciated area was initially defined by sets of uniform load areas which are defined by specific ranges of altitude or snow accumulation. In the second approach, it was defined by a unique area on which each pixel was given a load scale factor proportional to the *a priori* information on snow load at day 91 (April 1). This day corresponds to the minimum in vertical ground displacements derived from the forward modelling of the *a priori* snow information.

We began by inverting for loads using both the vertical and the horizontal components of the cGPS seasonal cycles. At each station, each component was given a weight inversely proportional to the squared standard deviation obtained when extracting the annual and semi-annual components. Furthermore, we experimented with imposing an additional weight factor of vertical relative to horizontal components. After trying different values for such a weight factor, we found more realistic inversion results by using only the vertical component. That approach was used throughout. The horizontal components are more sensitive to the geometry of the load distribution than the vertical component, but the spatial distribution of the cGPS stations is not well suited; the highest number of stations is in the southwest and central part of Iceland, in the middle of most of the loads. There could also be an underestimation of size of the horizontal component displacements when using a spherical elastic Earth model (Chanard *et al.* 2014; Kristel Chanard, private communication, 2015).

3.2 Original Earth models

The most simple load we tried inverting for was an uniform load over all of Iceland with thickness varying according to the time of year. As such, the inversion was setup to use whole Iceland as an area, and using the PREM Green's functions. Results (Fig. 9) show clear load increase during winter, with a maximum in May. Of the 72 inversions to infer a complete seasonal loading cycle (see above), the best-fitting model gives a maximum for the GPS up component weighted root mean squares (WRMS) of about 3.6 mm. It can be compared to the maximum of 9.5 mm for the up component WRMS in the data when no models are applied. The timing of the maximum and the shape of the inverted seasonal cycle is a clear indication that snow is the main seasonal load in Iceland. The geometry of this uniform load model is however quite unrealistic as we know that the distribution of snow fall in Iceland is not uniform over the whole country. A more detailed model is warranted.

In a more advanced approach, we inverted for combinations of the specific load areas: glaciers, the Hálslón reservoir, ocean, atmosphere and snow on non-glaciated areas. Glacier annual mass balance and ocean bottom pressure, which both are expected to have a seasonal cycle, were kept free in all model inversions. On the other hand, *a priori* information on the atmospheric load, snow load in non-glaciated areas and the Hálslón load was included to some degree in the inversion. When used, the expected displacements from a combination of these loads were subtracted prior to inversion. With this combination, inversion of the cGPS seasonal cycles allowed us to get good estimation of the ocean and glacier loads while being able to check for the consistency of the other loads with their *a priori* information.

At first, we investigated for the difference between various Earth models (Table 1). We used each of them for the inversion of the same set of loads and compared the results. Deformation induced by loads concentrated in a small area are expected to be governed by elastic properties at shallow depth (upper crust), while deformation induced by loads covering large areas are expected to be affected by deeper levels (lower part of the crust and the upper mantle). The Hálslón reservoir has a relatively small area and all the cGPS in the vicinity are next to the reservoir. Therefore, it probes best the upper crustal elastic parameters. The Hálslón seasonal load was very stable through all inversions with a minimum around mid-April and a maximum at the beginning of September. Its load estimate is fairly independent from the other estimated loads. Table 1 shows that the Gutenberg–Bullen model, the G-B continental shield model and the PREM model give similar inversion results in terms of rms and load value for Hálslón. The 1066A model results in a much smaller load value for Hálslón than the others. Comparison of the elastic moduli of the Earth models shows that the 1066A model has a Young modulus of about 37.5 GPa in the 11 topmost km of the crust (Fig. 7), lower than the other Earth models. Below that the 1066A model switches to a high Young modulus of about 170 GPa. All the other models have higher Young's modulus near the surface (70–85 GPa) and then progressively change towards higher values with depth, reaching the value of 170 GPa at 25–40 km depth.

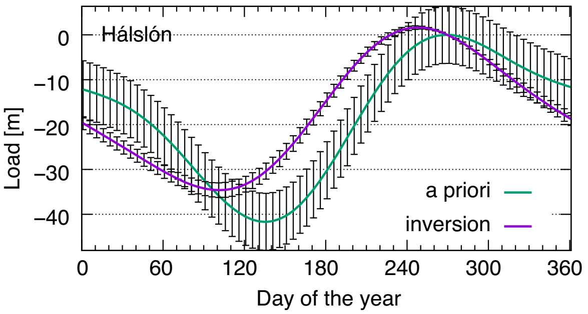

Figure 10. Seasonal cycles for Hálslón obtained from *a priori* information and from inverting the cGPS vertical seasonal cycles using the unscaled PREM model. Load is given in metres of water equivalent. Seasonal cycles are relative to day 270 of the year. Error bars show $1-\sigma$ standard deviation.

Although the properties of the topmost layer of the 1066A model are really similar to the one used by Grapenthin *et al.* (2006), it appears to be too soft to explain the Hálslón loading. When using the PREM model, the Hálslón seasonal cycle is very similar to the actual lake-level seasonal cycle. However, it is shifted by about 30 d earlier (Fig. 10). The seasonal cycle at cGPS sites near the Hálslón reservoir has important contributions not only from the reservoir, but also from glacial and snow loads that actually dominate the signal. Thus, the temporal shift may relate to some loss of information caused by using a combination of sine and cosine functions to describe the stations deformation seasonal cycle. Another possibility could relate to variation in the ground water level in the surrounding areas but further studies of that are needed.

When using any of the unscaled Earth models, glaciers, snow and atmosphere loads were overestimated (when compared to the *a priori* information available), implying that all of them were too rigid. All models have a similar Young's modulus below 40 km, a depth that will govern the influence of very extensive loads (Fig. 7). The particular location of Iceland, a hotspot on the Mid-Atlantic Ridge (e.g. Sigmundsson 2006), suggests that the upper mantle and crustal rigidity may be lower than the world average. The global models used in this study may therefore not be fully suited to describe the particular elastic moduli under Iceland. Here, we take the approach of scaling the inferred displacements from the original PREM Green's functions table to account for this difference in elastic moduli. This is a simple approximation for considering deviations from the PREM model for loads of limited size over Iceland. However, it implies a constant scaling of the elastic properties in the PREM model without possibilities to induce variations at specific depths.

3.3 Scaled PREM model

We started by running numerous inversions with various combinations of the loads using the original PREM model and compared the results. We found a scale factor of 2.3 ± 0.6 on values in the PREM Green's function table was necessary so that the glaciers load (Vatnajökull in particular) inferred from inversions was similar to available *a priori* information. *A priori* load information and selected inversions results are compared in Table 2 (see Appendix A for the loads seasonal cycles derived from selected inversions).

Because we only used the vertical component of the cGPS seasonal cycle in the inversion, ocean and atmosphere are strongly anticorrelated. The inverted atmosphere load seasonal cycle is similar to the seasonal cycle derived from the ERA-Interim data set. It has a minimum at the start of the year and a maximum three month later. Ocean inversion results show a load amplitude of 6 cm of water equivalent, with a trend similar to the GRACE data for the Arctic ocean. Even with such a small amplitude, ocean load has to be considered because it improves the atmospheric load results by minimizing its loading during fall.

The Hálslón seasonal cycle is similar to the previous results, except its amplitude was minimized because of the scale factor applied to the PREM.

When estimated independently, Mýrdalsjökull and Vatnajökull areas give fairly similar load seasonal cycles trough all inversions: loading from November until June and fast unloading the rest of the year. Vatnajökull had an amplitude of 170 ± 11 cm of SWE while Mýrdalsjökull had an amplitude of 172 ± 25 cm of SWE ($m_{3\text{glaciers}}$ in Table 2). The Langjökull and Hofsjökull load was very sensitive to the other loads in the inversion process. Results show that this load has a similar trend as the Mýrdalsjökull and Vatnajökull loads. However, the load maximum happens earlier in the spring and the load amplitude is almost twice as large as the expected one. The location of these ice caps in the central part of Iceland and the absence of cGPS north of them could be an explanation. Because of this inconsistency in the load estimates when glaciers are independent, we consider the most appropriate approach to take all the ice

Table 2. Comparison of the amplitude of inverted loads seasonal cycles with other data sets.

Source	Vatnajökull	Mýrdalsjökull	Langjökull	Hofsjökull	Snow	Atmosphere	Hálslón	Ocean
Grapenthin *et al.* (2006)	150	∼250	165	125	–	–	–	–
Personal communication[a]	151 ± 26	–	170 ± 37	–	–	–	–	–
This study (IMO model)	–	–	–	–	0.243 ± 40	–	–	–
This study (ERA-Interim)	–	–	–	–	–	14.4 ± 13.5	–	–
This study (Landsvirkjun)	–	–	–	–	–	–	4172 ± 636	–
m_{Best} (Fig. 11)	*147 ± 10	*245 ± 17	*165 ± 11	*122 ± 8	*r*	23.4 ± 3.2	–	6.3 ± 1.6
m_{rAtmo} (Fig. A1)	*152 ± 7	*253 ± 12	*171 ± 8	*127 ± 6	*r*	*r*	–	11 ± 1
m_{Snow} (Fig. A2)	*156 ± 10	*260 ± 16	*176 ± 11	*130 ± 8	0.59 ± 0.06[b]	11 ± 5.8	–	6.2 ± 1.3
$m_{Halslon}$ (Fig. A3)	*149 ± 10	*249 ± 17	*168 ± 11	*125 ± 8	*r*	23.5 ± 3.5	1764 ± 97	6.5 ± 1.6
$m_{2\text{Glaciers}}$ (Fig. A4)	162 ± 11	*186 ± 26	*127 ± 18	*93 ± 13	*r*	23.6 ± 3.2	–	6.3 ± 1.6
$m_{3\text{Glaciers}}$ (Fig. A5)	170 ± 11	172 ± 25	*311 ± 57	*236 ± 43	*r*	24.1 ± 4.3	–	4.4 ± 1.3

[a]Personal communication with Finnur Pálsson, University of Iceland. Based on annual summer and winter mass balance measurements between 2014 and 2015.

[b]Fraction of the *a priori* snow load information on day 91 relative to day 270.

*This glacier load is proportional to the other glacier loads marked with *. Proportion between glaciers is derived from the *a priori* information on their load amplitudes (see the text).

r: Displacements derived from the *a priori* load information were removed before inversion.

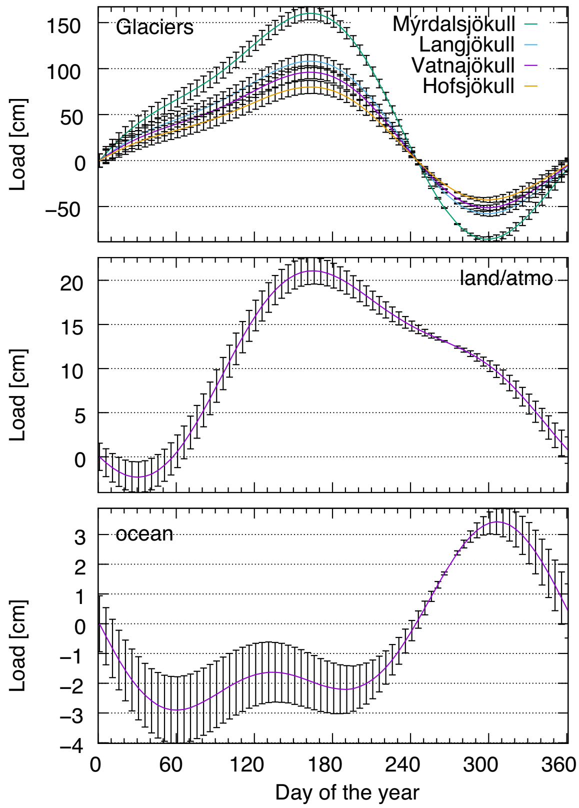

Figure 11. Seasonal cycle for glaciers, atmosphere and ocean loads obtained from inverting the cGPS vertical seasonal cycles using the PREM Green's function scaled by 2.3. Glaciers loads were inverted as a unique load with a preset internal load scale factor according to the ratio of their *a priori* mass balances (see the text). Effects from snow load in non-glaciated areas are removed before inversion and stations close to Hálslón are not included. Load is given in centimetres of water equivalent. Seasonal cycle is relative to the January 1. Error bars show $1-\sigma$ standard deviation. Load results and their associated areas (Fig. 8) are available at the FUTUREVOLC data hub (see Acknowledgments).

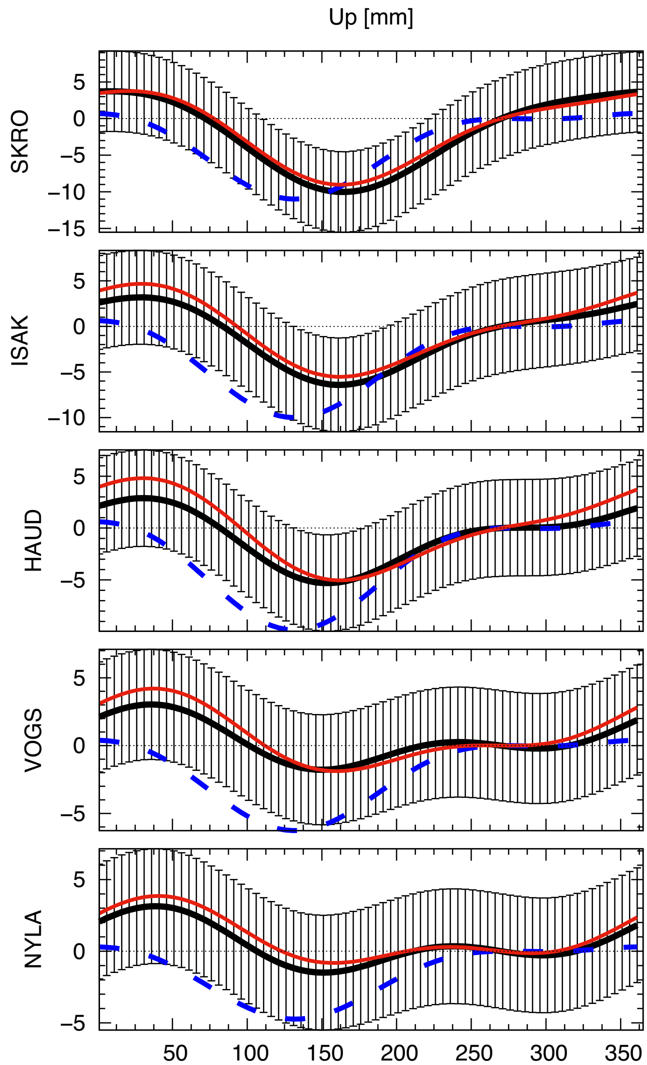

Figure 12. Comparison between vertical seasonal cycles: estimated from cGPS time-series (thick black line), calculated from the 1-load model (blue dashed line) and calculated from the $m_{\rm Best}$ model (red line). Errors bars show $1-\sigma$ standard deviation of the GPS stations seasonal cycle. cGPS sites are the same as in Fig. 2.

caps as one load, with preset relative load factors between the ice caps (as described above).

Inversion for the snow load in non-glaciated areas gave best results when each pixel of the snow area was given a scale factor proportional to the *a priori* information on snow load at day 91. Attempts were also made to invert for snow load by dividing the area into subareas with a similar range of altitude or similar range of snow load in April. The altitude range from 1050 to 2000 m and the range from 700 to 1050 were the most relevant but inversion results were not satisfactory. An explanation may be that although the snow accumulation data show some correlation with altitude, there is important difference between the west and east of Iceland. The snow load ranges, considering the relative amount of snow in the areas at day 91, gave better results than the altitude ranges. However, both altitudes ranges and snowfall ranges show a larger load amplitude at medium altitude/snowfall ranges than high altitude/snowfall ranges. This could be caused by the limited number of cGPS at high altitude and in areas with heavy snow accumulation.

Best load results were obtained when inverting for three loads: (i) glaciers (as one load with predefined load scale factor between glaciers), (ii) atmosphere and (iii) ocean loads, with snow load in non-glaciated area removed beforehand and excluding sites near Hálslón (Fig. 11, $m_{\rm Best}$ in Table 2). This model gives a realistic glacier load seasonal cycle and reproduces well the *a priori* information on the seasonal cycle of the atmosphere load with the exception of a larger amplitude. Ocean load was considered because its removal would strongly affect the atmospheric load amplitude and seasonal cycle aspect. The maximum WRMS are found in spring when the displacements are at their maximum: 1.46, 1.61 and 1.93 mm for the east, north and up components, respectively. Fig. 12 compares the up component seasonal cycle derived from time-series at given cGPS sites with the inversion results from the uniform load model and the $m_{\rm Best}$ model. The $m_{\rm Best}$ model is a clear improvement over the uniform load model and reproduces fairly well the cGPS seasonal cycles. The derived seasonal cycles from this inversion is within the standard deviation of the cGPS seasonal cycles and maximum residual is less than 2 mm.

3.4 Load contribution to observed displacements

We estimated the contribution of each load considered in the $m_{\rm Best}$ inversion, in which the scaled version of the PREM Green's

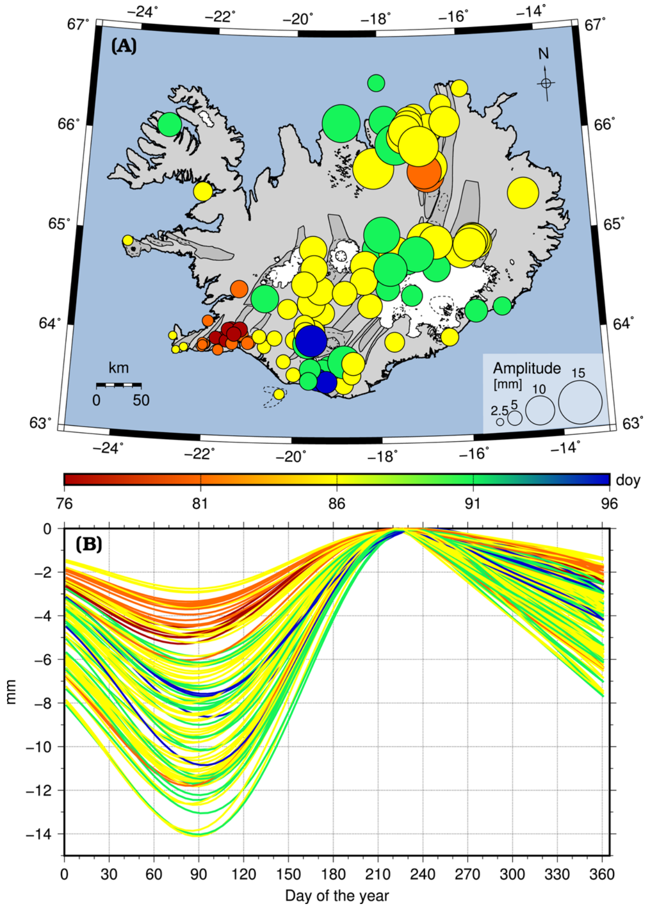

Figure 13. Inferred seasonal cycle of the vertical deformation induced by snow loading in non-glaciated area (as shown on Fig. 4) at each cGPS site using the PREM Green's function scaled by 2.3. (A) Time of minimum and amplitude of the estimated seasonal cycle of the vertical deformation. Circles show data points: size shows the amplitude of the seasonal signal and colour shows the day of the year of the minimum. (B) Seasonal cycle at each cGPS site with the same colour scale as in (A). Each seasonal cycle is shown relative to its maximum.

function was used. Prior to inversion, we removed the contribution of the snow on non-glaciated area based on its *a priori* information. Induced seasonal vertical displacements due to snow on non-glaciated areas are highest in the central part of north Iceland, with amplitudes up to 14 mm (Fig. 13). Amplitudes range from 5 to 10 mm near the glaciers as well as in the centre and in the NW of Iceland, but only 1–2 mm on the Reykjanes peninsula. Induced horizontal displacements are towards an area east of Hofsjökull with amplitudes of about 2 mm near the coast and close to zero in the central part of Iceland. Glaciers, atmosphere and ocean load seasonal cycle were derived from the inversion. Glacier loading induces vertical displacement of 22 mm at a site in the centre of the Vatnajökull ice cap. Amplitude of the vertical displacements then decreases with distance away from the ice caps, down to 1 mm in the Westfjords. Horizontal displacements are towards the centre of the Vatnajökull ice cap, with exception of sites really close to some of the other ice caps. Displacements range from less than 1 mm in the Westfjords and the Reykjanes peninsula, up to more than 3 mm at the sites near the edge of the Vatnajökull ice cap. Atmospheric loading induces vertical displacements with amplitudes of 7–8 mm inland and 3–4 mm near the coast line. Horizontal displacements are towards the east side of Hofsjökull from where their amplitudes start increasing gradually with the distance away from it, up to 2 mm for sites near the coastline. The ocean contribution is fairly homogeneous over Iceland with vertical displacements of a 3 mm near the coast and 2 mm inland. This is about an order of magnitude smaller than the contribution of the snow load and an order of magnitude smaller than the seasonal cGPS vertical cycle. The horizontal displacements are insignificant.

The atmosphere load seasonal cycle derived from inversion reproduces very well the one derived from *a priori* information but it has a larger amplitude. The seasonal cycle derived from *a priori* information would generate a similar pattern of deformation but with reduced amplitude: 1–2 to 3–4 mm in the vertical and less than a millimetre in the horizontal.

The Hálslón load was not considered in the previous inversion as we excluded the nearby cGPS sites. However, it still generates local but important deformation on its surrounding areas. Inversion with the non-modified PREM Green's function table gives a reservoir seasonal cycle fairly similar to what the *a priori* data are showing (Table 1). Using this model, the nearby cGPS move up to more than 20 mm in the vertical and 5 mm in the horizontal, depending on their distance to the reservoir.

4 DISCUSSION

The data presented here and our modelling show that snow loading on glaciers (glacier mass balance) as well as non-glaciated areas are the main contributor to the seasonal deformation in Iceland. We present an improved model of the effect of snow loading when compared to the work of Grapenthin *et al.* (2006), who only considered glacier mass balance. There is no sign of non-elastic ground response to seasonal loading. Snow loading in areas outside glaciers has a major influence on ground deformation seasonal cycle in other places than Iceland. The effect has, for example, been well documented in Japan (Heki 2004) and Alaska (Fu *et al.* 2012). The timing of the snow loading is different in these areas: maximum in March in Japan, April in Alaska and in May in Iceland. The minimum in the vertical seasonal cycle in these areas occurs at a very similar time as the snow load maximum in its surroundings. Similarly, stations close to glaciers are continuously showing signs of loading or unloading while stations further away show it mostly for the local snow time period (Fig. 2). Deviation from this pattern in the timing of the minimum is observed at a number of cGPS stations (Fig. 3). Sites near Hálslón are strongly influenced by the reservoir loading which has the opposite phase to the snow loading. The ISAF station in the Westfjords area in the NW-Iceland has the earliest minimum of all stations. It can be explained by the fact that this station is the furthest away from the main ice caps, Vatnajökull in particular, making their loading influence small compared to the Westfjords snow influence. The GMEY station, located on the Grímsey island in the Arctic Ocean, has its minimum as late as the station in the middle of Vatnajökull, which is the most affected by glacier loading. Local ocean loading may be an explanation for this late minimum.

Deviations from the estimated seasonal cycle are observed in each data set. These deviations can last from a few weeks to more than a year. Starting in mid-2007 and stopping around fall 2008, there is an important downward deviation seen on most cGPS, especially in SW-Iceland (Fig. 14). The pattern can be explained by additional loading occurring in the second half of 2007 and the unloading in the middle of 2008. According to the Icelandic Meteorological Office (2015), the second half of 2007 was among the wettest ever registered in the south and west of Iceland, and 2008 began with heavy precipitation. The following summer was very dry. We infer

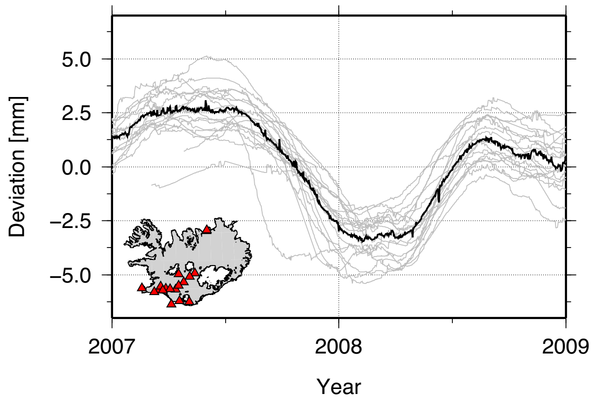

Figure 14. Deviation of GPS vertical time-series from best-fitting curves using eq. (1) in the 2007–2008 period. Grey lines show deviation for each selected GPS stations, thick black line shows average deviation. Bottom-left corner: map of Iceland with red triangle showing location of selected GPS sites.

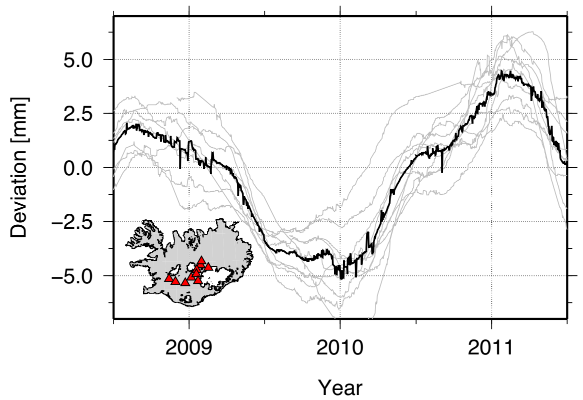

Figure 15. Same as Fig. 14 for the period from middle of 2008 to middle of 2011.

that this unusual precipitation pattern did induce extra loading by snow and/or ground water and caused more ground subsidence than usual. The unloading occurred at the same time as the usual snow melt. This reinforces our idea that this deviation was the effect of unusually high snow accumulation.

Another important period of (downward) vertical deviation occurs from the beginning of 2009 until the end 2010. It is clearly visible on stations in the central part of Iceland (Fig. 15), and can even be detected on most of cGPS stations. The signal, and inferred additional loading, happens mainly during the second quarter of 2009 and the unloading starts at the beginning of 2010 and lasts until the end of the same year. The observed average displacement from the unloading almost reaches a centimetre and is twice as large as the average loading displacement. As reported by the Icelandic Meteorological Office (2015), the second quarter of 2009 was particularly wet. We think that this weather led to extra snowfall on the ice caps, inducing extra loading. The IMO says that 2010 was one of the warmest and driest year on record and the snowfall was unusually light. The snow load data from IMO show also low accumulation in winter 2009–2010. This could be related to the winter 2009–2010 record-breaking Arctic oscillation which led to unusual weather conditions in the Arctic region (Matsuo & Heki 2012). At the same time, glacier mass balance measurements show a very high mass loss in 2010 with melting enhanced by volcanic ash from the 2010 Eyjafjallajökull eruption (Björnsson *et al.* 2013). This indicates that the unloading was caused by a lack of snow during winter in addition to an unusually high mass loss from the glaciers. Some other deviations from the seasonal GPS cycle seem to be related to atmospheric pressure deviation.

In order to validate the approximation of describing load seasonal variation by a combination of two sine and two cosine functions, we compared the inversion results after the removal of the snow load effect estimated in two different ways. In the first one, we used the snow load values given by the sine and cosine functions to calculate the induced displacements and remove them before running the inversion. In the second case, the snow load values were given by a 5-day average over the course of one year. Inversion results showed very little differences in both the trend and amplitude of the loads. This indicates that there was no issue with describing the snow load seasonal variation with sine and cosine functions. This approximation can, however, be bypassed when inverting directly for the observed time-series instead of an averaged year (e.g. Compton *et al.* 2015b).

Inversion statistics show a strong anticorrelation between the ocean load and the atmosphere load. This is a consequence of using only the vertical GPS component in the inversion of such large uniform loads. The ocean seasonal cycle derived from the inversion has a trend similar to the seasonal gravity anomaly in the Arctic Ocean. Using the horizontal component of the deformation in the inversion would help to discriminate the atmosphere and ocean loads. We could also get additional information about the ocean load distribution around Iceland and compare it with the non-uniform load distribution shown by the GRACE data.

A summary of the inversion setups and results is shown in Table 2. Model m_{rAtmo} shows that removing the estimated atmospheric load displacements before inversion influences the ocean load estimation but has very little influence on the glaciers load estimation. Estimating the snow load instead of removing its effect derived from *a priori* information before inversion influences mainly the atmospheric load estimation (model m_{Snow}). Excluding the cGPS sites near the Hálslón water reservoir does not change the inversion results for the other loads (model m_{Halslon}). Glacier inversion results are very sensitive to inverting for independent sets of glaciers instead of a unique scaled one. In model $m_{\mathrm{2Glaciers}}$, the Vatnajökull load remains close its *a priori* information while the Mýrdalsjökull, Langjökull and Hofsjökull loads are underestimated. This could be an indication that the crust and mantle are more rigid under Mýrdalsjökull, Langjökull and Hofsjökull than under Vatnajökull. However, model $m_{\mathrm{3Glaciers}}$ shows us that when Vatnajökull and Mýrdalsjökull are separate they have similar load estimate (overestimation for Vatnajökull and underestimation for Mýrdalsjökull) while Langjökull and Hofsjökull are overestimated by a factor of two.

The temporal pattern of the inferred glacier load seasonal cycle has the expected trend: fast unloading in summer and gradual snow loading through the winter and the spring. However, all the glacier loads are overestimated without applying a scale factor of 2.3 to the PREM Green's function table. This in an indication that the upper rigidity of the model is too high compared to the actual values beneath Iceland. The ratio between the inverted and expected load amplitude is different between ice caps when they are estimated independently. This could be caused by lateral variation of Earth elastic properties or an issue with the distribution of the cGPS stations around the ice caps. The latter issue is most likely an important factor in the overestimation of the Langjökull and Hofsjökull load. Moreover, the sensitivity of this load to the snow load and atmospheric load reflects that its central location in Iceland is influencing the inversion process.

According to the inversion results, the PREM fails to describe properly the Icelandic crust and upper-mantle elastic properties. The top part, constrained by smaller loads like Hálslón, shows elastic properties close to the Icelandic ones but slightly too soft. The deeper part of the model, constrained by the glacier load, shows that the model is too rigid: a 2.3 ± 0.6 scale factor needs to be applied to the PREM Green's function. This indicates a lower rigidity under Iceland than elsewhere which can be explained by the tectonic setting of Iceland: a hotspot on an active mid-oceanic ridge. This generates anomalously high temperatures in the mantle, which are then likely to lower its rigidity (Jackson *et al.* 2007). Increased mantle melting caused by the mantle plume (Ito *et al.* 1999) could also contribute to lower the overall rigidity under Iceland. Lower elastic moduli than the world average is not restricted to hotspots can also be found in some other tectonic settings (e.g. Ito & Simons 2011). A lateral variation of the elastic moduli is also to be expected in Iceland (Wolfe *et al.* 1997; Bjarnason & Schmeling 2009), and could be considered in further modelling. The approach taken here to scale the PREM Green's functions is simple and implies constant scaling of elastic properties at depths sensitive to the loading. A more correct approach would be to recompute the Green's functions for a revised Earth model considering not only constant scaling of elastic properties, but also variable scaling for specific depth intervals. Such a study was beyond the scope of our work but is worth further investigation. The revised Earth model would make it viable to invert directly from the time-series instead of their inferred seasonal cycle terms. The current deviation of the cGPS seasonal cycle could then be directly explained during the inversion process. Considering the use of the horizontal component of the seasonal cycles would also help the discrimination of loads influence, especially the atmospheric and oceanic ones.

5 CONCLUSIONS

Time-series of position of 71 cGPS stations in Iceland include an annual and semi-annual cycle, ranging in amplitude in the vertical from 4 mm near the coastline up to 27 mm at the centre of the Vatnajökull ice cap, and up to 6 mm in the horizontal. The cycle is well explained as an Earth response to loads considering a combination of the annual mass balance of glaciers, snow load on non-glaciated areas, Hálslón lake reservoir changes, response to on-land seasonal variation in pressure and oceanic loading. Using a layered isotropic spherical Earth model and inverting the cGPS vertical seasonal cycle in terms of the load components, *a priori* information on load seasonal cycles (snow, atmosphere and Hálslón) can be reproduced and an estimate of the seasonal cycle of other loads (glaciers and ocean) can be derived. Displacements induced by variations in the smallest load, Hálslón, are well fit using the PREM Earth model. For wider loads, best results are obtained when using the PREM scaled by a factor of 2.3, consistent with the low effective rigidity at depth under Iceland. Using this scale factor and removing the effects of snow loading in non-glaciated areas, and excluding stations close to Hálslón, allows a realistic inversion for glaciers, atmospheric and ocean loads. It shows that seasonal glacier mass balance and snow on non-glaciated areas contributes the most to the seasonal deformation, over 10 mm in many locations in Iceland, but also that the rest of the deformations can be explained by a combination of atmosphere, ocean and reservoir loads. Interannual deviations in the observed ground displacements are correlated with unusual temperature, precipitation and atmospheric pressure. A revised Earth model, with more realistic variation in elastic moduli, is needed to further improve the quality of the inversion results. This model, combined with more extended GPS observations, could make it possible to derive daily estimates of the various loads considered here (glaciers, snow, atmosphere, ocean and Hálslón).

ACKNOWLEDGEMENTS

We wish to thank Nikolai Nawri and Tómas Jóhannesson from the Icelandic Meteorological Office for providing the snow data and comments on their interpretation in ice-free and glacier-covered areas, Landsvirkjun for providing the Hálslón lake-level data, the European Centre for Medium-Range Weather Forecasts (ECMWF) for providing the ERA-Interim data and the Center for Space Research (University of Texas, USA) for providing the GRACE data. Data were downloaded from following URLs, ERA-interim: http://apps.ecmwf.int/datasets/data/interim-full-daily/, GRACE: ftp://podaac.jpl.nasa.gov/allData/grace/L2/CSR/RL05 We would like to thank Finnur Pálsson and Helgi Björnsson at the Institute of Earth Sciences, University of Iceland, for providing us with glacier mass balance data and helpful comments. This research was partly supported by the Watanabe Trust Fund for a 5-months visit at Hokkaido University, the European Community's Seventh Framework Programme grant no. 308377 (Project FUTUREVOLC) and Landsvirkjun. We would like to thank the Icelandic Meteorological Office for maintaining the cGPS network. Instruments were financed by various institutions including the International GNSS Service (IGS), the National Land Survey of Iceland, the University of Savoie (France), the University of Arizona (USA), the Institute of Earth Sciences of University of Iceland, the Nordic Volcanological center, the ETH Zurich (Switzerland), the Pennsylvania State University (USA) and the Bavarian Academy of Sciences and Humanities (Germany). The Central Highlands Iceland (CHIL) GPS network was funded by the University of Arizona and grants from NSF (EAR-0711446 to the University of Arizona) and the Icelandic Center for Research RANNIS (60243011 to the Nordic Volcanological Center, University of Iceland). Load inversion results from best-fitting model and their associated areas, as well as most of the GPS RINEX data set are available at the FUTUREVOLC data hub http://futurevolc.vedur.is. However, few GPS stations are being used for student projects and these will only be available thereafter. Few other GPS stations operated by Pennsylvania State University (USA) are also not in the data hub. Figures were produced with the GMT software (Wessel & Smith 1998) and Gnuplot.

REFERENCES

Alterman, Z., Jarosch, H. & Pekeris, C.L., 1961. Propagation of Rayleigh waves in the Earth, *Geophys. J. Int.,* **4,** 219–241.

Auriac, A., Spaans, K.H., Sigmundsson, F., Hooper, A., Schmidt, P. & Lund, B., 2013. Iceland rising: solid Earth response to ice retreat inferred from satellite radar interferometry and visocelastic modeling, *J. geophys. Res.,* **118,** 1331–1344.

Árnadóttir, T., Lund, B., Jiang, W., Geirsson, H., Björnsson, H. & Einarsson, P., 2009. Glacial rebound and plate spreading: results from the first countrywide GPS observations in Iceland, *Geophys. J. Int.,* **177,** 691–716.

Auriac, A., Sigmundsson, F., Hooper, A., Spaans, K.H., Björnsson, H., Pálsson, F., Pinel, V. & Feigl, K.L., 2014. InSAR observations and models of crustal deformation due to a glacial surge in Iceland, *Geophys. J. Int.,* **198,** 1329–1341.

Bennett, R.A., 2008. Instantaneous deformation from continuous GPS: contributions from quasi-periodic loads, *Geophys. J. Int.,* **174,** 1052–1064.

Bjarnason, I.T. & Schmeling, H., 2009. The lithosphere and asthenosphere of the Iceland hotspot from surface waves, *Geophys. J. Int.,* **178,** 394–418.

Björnsson, H. *et al.*, 2013. Contribution of Icelandic ice caps to sea level rise: trends and variability since the Little Ice Age, *Geophys. Res. Lett.,* **40,** 1546–1550.

Chanard, K., Avouac, J.P., Ramillien, G. & Genrich, J., 2014. Modeling deformation induced by seasonal variations of continental water in the Himalaya region: sensitivity to Earth elastic structure, *J. geophys. Res.,* **119**(6), 5097–5113.

Compton, K., Bennett, R. & Hreinsdóttir, S., 2015a. Climate driven vertical acceleration of Icelandic crust measured by CGPS geodesy, *Geophys. Res. Lett.*, **42**(3), 743–750.

Compton, K., Bennett, R., Hreinsdóttir, S., van Dam, T. & Spada, G., 2015b. CGPS as a tool to measure short-term mass balance variations of Icelandic ice caps, in *AGU Fall Meeting,* 14–18 December 2015, American Geophysical Union.

Decriem, J. *et al.*, 2010. The 2008 May 29 earthquake doublet in SW Iceland, *Geophys. J. Int.,* **181,** 1128–1146.

Dee, D.P. *et al.*, 2011. The ERA-Interim reanalysis: configuration and performance of the data assimilation system, *Q. J. R. Meteorol. Soc.,* **137**(656), 553–597.

Dziewonski, A.M. & Anderson, D.L., 1981. Preliminary reference Earth model, *Phys. Earth planet. Inter.,* **25**(4), 297–356.

Farrrell, W.E., 1972. Deformation of the Earth by surface loads, *Rev. Geophys. Space Phys.,* **10,** 761–797.

Fu, Y., Freymueller, J.T. & Jensen, T., 2012. Seasonal hydrological loading in southern Alaska observed by GPS and GRACE, *Geophys. Res. Lett.,* **39,** L15310, doi:10.1029/2012GL052453.

Geirsson, H. *et al.*, 2006. Current plate movements across the Mid-Atlantic Ridge determined from 5 years of continuous GPS measurements in Iceland, *J. geophys. Res.,* **111,** B09407, doi:10.1029/2005JB003717.

Geirsson, H. *et al.*, 2010. Overview of results from continuous GPS observations in Iceland from 1995 to 2010, *Jökull,* **60,** 1–21.

Gilbert, F. & Dziewonski, A.M., 1975. An application of normal mode theory to the retrieval of structural parameters and source mechanisms from seismic spectra, *Phil. Trans. R. Soc. A,* **278,** 187–269.

Grapenthin, R., Sigmundsson, F., Geirsson, H., Árnadóttir, T. & Pinel, V., 2006. Icelandic rhythmics: annual modulation of land elevation and plate spreading by snow load, *Geophys. Res. Lett.,* **33**, doi:10.1029/2006GL028081.

Guo, J.Y., Li, Y.B., Huang, Y., Deng, H.T., Xu, S.Q. & Ning, J.S., 2004. Green's function of the deformation of the Earth as a result of atmospheric loading, *Geophys. J. Int.,* **159,** 53–68.

Harkrider, D.G., 1970. Surface waves in multilayered elastic media. Part II. Higher mode spectra and spectral ratios from point sources in plane layered Earth models, *Bull. seism. Soc. Am.,* **60,** 1937–1987.

Heki, K., 2001. Seasonal modulation of interseismic strain buildup in northeastern Japan driven by snow loads, *Science,* **293,** 89–92.

Heki, K., 2004. Dense GPS array as a new sensor of seasonal changes of surface loads, in *The State of the Planet: Frontiers and Challenges in Geophysics,* pp. 177–196, eds Sparks, R.S.J. & Hawkesworth, C.J., American Geophysical Union, Washington, DC.

Heki, K. & Matsuo, K., 2010. Coseismic gravity changes of the 2010 earthquake in central Chile from satellite gravimetry, *Geophys. Res. Lett.,* **37** (24), doi:10.1029/2010GL045335.

Hreinsdóttir, S., Árnadóttir, T., Decriem, J., Geirsson, H., Tryggvason, A., Bennett, R.A. & LaFemina, P., 2009. A complex earthquake sequence captured by the continuous GPS network in SW Iceland, *Geophys. Res. Lett.,* **36,** L12309, doi:10.1029/2009GL038391.

Icelandic Meteorological Office 2015. Annual weather articles. Available at: http://en.vedur.is/climatology/articles/annual/, last accessed 20 January 2016.

Ito, G., Shen, Y., Hirth, G. & Wolfe, C.J., 1999. Mantle flow, melting, and dehydration of the Iceland mantle plume, *Earth planet. Sci. Lett.,* **165,** 81–96.

Ito, T. & Simons, M., 2011. Probing asthenospheric density, temperature, and elastic moduli below the Western United States, *Science,* **332,** 947–951.

Jackson, J.M., Sinogeikin, S.V. & Bass, J.D., 2007. Sound velocities and single-crystal elasticity of orthoenstatite to 1073 K at ambient pressure, *Phys. Earth planet. Inter.,* **161,** 1–12, doi:10.1016/j.pepi.2006.11.002.

Jóhannesson, H. & Sæmundsson, K., 2009. *Geological Map of Iceland*, Tectonics, Icelandic Institute of Natural History.

Lyard, F., Lefevre, F., Letellier, T. & Francis, O., 2006. Modelling the global ocean tides: modern insights from FES2004, *Ocean Dyn.,* **56,** 394–415.

Matsuo, K. & Heki, K., 2012. Anomalous precipitation signatures of the Arctic Oscillation in the time-variable gravity field by GRACE, *Geophys. J. Int.,* **190,** 1495–1506.

Okubo, S. & Saito, M., 1983. Partial derivative of love numbers, *Bull. Geod.,* **57,** 167–179.

Pinel, V., Sigmundsson, F., Sturkell, E., Geirsson, H., Einarsson, P., Gudmundsson, M.T. & Högnadóttir, T., 2007. Discriminating volcano deformation due to magma movements and variable surface loads: application to Katla subglacial volcano, Iceland, *Geophys. J. Int.,* **169,** 325–338.

Seity, Y., Brousseau, P., Malardel, S., Hello, G., Bénard, P., Bouttier, F., Lac, C. & Masson, V., 2011. The AROME-France convective-scale operational model, *Mon. Weather Rev.,* **139,** 976–991.

Sigmundsson, F., 2006. *Iceland Geodynamics Crustal Deformation and Divergent Plate Tectonics,* Praxis Publishing, Springer Verlag.

Sigmundsson, F. *et al.*, 2010. Intrusion triggering of the 2010 Eyjafjallajökull explosive eruption, *Nature,* **468,** 426–430.

Sigmundsson, F. *et al.*, 2014. Segmented lateral dyke growth in a rifting event at Bárðarbunga volcanic system, Iceland, *Nature,* **517,** 191–195.

Swenson, S. & Wahr, J., 2006. Post-processing removal of correlated errors in GRACE data, *Geophys. Res. Lett.,* **33,** L08402, doi:10.1029/2005GL025285.

Tregoning, P. & van Dam, T., 2005. Atmospheric pressure loading corrections applied to GPS data at the observation level, *Geophys. Res. Lett.,* **32,** L22310, doi:10.1029/2005GL024104.

Tregoning, P. & Watson, C., 2009. Atmospheric effects and spurious signals in GPS analyses, *J. geophys. Res.,* **114,** B09403, doi:10.1029/2009JB006344.

van Dam, T.M., Blewitt, G. & Heflin, M.B., 1994. Atmospheric pressure loading effects on Global Positioning System coordinate determinations, *J. geophys. Res.,* **99,** 23 939–23 950.

Wahr, J., Molenaar, M. & Bryan, F., 1998. Time variability of the Earth's gravity field: hydrological and oceanic effects and their possible detection using GRACE, *J. geophys. Res.,* **103,** 30 205–30 229.

Wessel, P. & Smith, W. H.F., 1998. New, improved version of generic mapping tools released, *EOS, Trans. Am. geophys. Un.,* **79,** 579, doi:10.1029/98EO00426.

Wolfe, C.J., Bjarnason, I.T., Vandecar, J.C. & Solomon, S.C., 1997. Seismic structure of the Iceland mantle plume, *Nature,* **385,** 245–247.

Zhang, Z.-Z., Chao, B.F., Lu, Y. & Hsu, H.-T., 2009. An effective filtering for GRACE time-variable gravity: fan filter, *Geophys. Res. Lett.,* **36,** L17311, doi:10.1029/2009GL039459.

Zhu, Y.S., Massmann, F.-H., Yu, Y. & Reigber, C., 2003. Satellite antenna phase center offsets and scale errors in GPS solutions, *J. Geod.,* **76**(11), 668–672.

APPENDIX A: SEASONAL CYCLE ESTIMATES AND OTHER INVERSIONS RESULTS

Table A1. Best-fitting annual and semi-annual components of the seasonal cycle for each cGPS sites.

	Annual		Semi-annual	
Site	Cosine	Sine	Cosine	Sine
AKUR	0.80 ± 0.14	−4.52 ± 0.14	0.68 ± 0.14	2.14 ± 0.14
ARHO	1.50 ± 0.12	−2.02 ± 0.12	0.33 ± 0.12	2.08 ± 0.12
BALD	5.32 ± 0.18	−5.39 ± 0.17	−0.02 ± 0.17	1.60 ± 0.18
BRUJ	5.54 ± 0.24	−5.06 ± 0.21	−0.26 ± 0.22	1.06 ± 0.22
BUDH	3.75 ± 0.13	−4.07 ± 0.13	0.42 ± 0.12	1.70 ± 0.13
DYNC	6.22 ± 0.18	−7.84 ± 0.18	−1.25 ± 0.17	1.27 ± 0.18
FEDG	3.58 ± 0.24	−4.32 ± 0.24	0.55 ± 0.23	1.48 ± 0.24
FITC	3.14 ± 0.19	−7.04 ± 0.18	0.38 ± 0.18	1.40 ± 0.18
FJOC	5.03 ± 0.18	−5.38 ± 0.17	0.06 ± 0.17	1.93 ± 0.17
FTEY	1.51 ± 0.16	−4.29 ± 0.18	0.76 ± 0.17	2.83 ± 0.16
GAKE	1.27 ± 0.19	−1.72 ± 0.20	0.24 ± 0.19	2.52 ± 0.19
GFUM	5.38 ± 0.51	−9.29 ± 0.37	−4.69 ± 0.44	2.15 ± 0.36
GLER	2.64 ± 0.16	−2.63 ± 0.17	−0.03 ± 0.15	1.33 ± 0.16
GMEY	1.76 ± 0.15	−0.86 ± 0.15	−0.43 ± 0.15	0.76 ± 0.15
GOLA	5.02 ± 0.19	−4.49 ± 0.19	−0.43 ± 0.18	1.24 ± 0.19
GRAN	0.43 ± 0.21	−3.48 ± 0.22	−0.68 ± 0.21	1.63 ± 0.21
GRVA	4.42 ± 0.18	−5.60 ± 0.17	0.64 ± 0.17	2.18 ± 0.17
HAMR	2.11 ± 0.25	−2.11 ± 0.23	0.06 ± 0.24	1.24 ± 0.24
HAUC	6.23 ± 0.14	−6.39 ± 0.14	0.42 ± 0.14	1.60 ± 0.14
HAUD	2.39 ± 0.13	−3.39 ± 0.14	0.35 ± 0.13	1.73 ± 0.13
HEDI	1.21 ± 0.17	−2.27 ± 0.17	0.43 ± 0.17	1.64 ± 0.17
HEID	1.93 ± 0.20	−4.11 ± 0.20	0.91 ± 0.20	2.10 ± 0.20
HEKR	4.54 ± 0.19	−4.13 ± 0.20	0.57 ± 0.20	1.12 ± 0.19
HESA	2.59 ± 0.19	−4.80 ± 0.20	0.83 ± 0.19	1.59 ± 0.20
HLFJ	2.19 ± 0.12	−3.20 ± 0.12	0.32 ± 0.12	1.39 ± 0.12
HLID	1.28 ± 0.11	−2.43 ± 0.11	0.76 ± 0.11	1.47 ± 0.11
HOFN	3.04 ± 0.10	−3.35 ± 0.10	0.12 ± 0.10	1.32 ± 0.10
HOTJ	1.84 ± 0.18	−3.14 ± 0.18	1.01 ± 0.18	2.41 ± 0.18
HVEL	3.51 ± 0.19	−3.55 ± 0.18	0.06 ± 0.18	2.29 ± 0.18
HVER	1.09 ± 0.10	−2.38 ± 0.10	0.53 ± 0.10	1.38 ± 0.10
HVOL	3.14 ± 0.12	−4.54 ± 0.12	0.08 ± 0.12	1.35 ± 0.12
INSK	4.31 ± 0.25	−3.91 ± 0.24	0.68 ± 0.23	2.18 ± 0.22
INTA	4.98 ± 0.16	−0.54 ± 0.17	0.20 ± 0.16	0.66 ± 0.17
ISAF	0.71 ± 0.24	−3.05 ± 0.22	1.56 ± 0.23	1.33 ± 0.23
ISAK	3.23 ± 0.11	−3.71 ± 0.11	0.14 ± 0.11	1.47 ± 0.11
JOKU	6.04 ± 0.16	−6.72 ± 0.16	0.49 ± 0.16	2.24 ± 0.16
KALF	4.20 ± 0.21	−4.11 ± 0.23	−0.21 ± 0.21	1.71 ± 0.22
KALT	1.68 ± 0.11	−1.73 ± 0.11	0.60 ± 0.11	1.31 ± 0.11
KARV	3.65 ± 0.18	0.28 ± 0.19	−0.33 ± 0.18	1.13 ± 0.18
KIDC	5.30 ± 0.15	−5.32 ± 0.15	0.02 ± 0.15	1.46 ± 0.15
KIDJ	1.89 ± 0.09	−1.91 ± 0.09	0.57 ± 0.09	1.30 ± 0.09
KOSK	0.15 ± 0.16	−1.65 ± 0.17	−0.05 ± 0.17	2.51 ± 0.16
KRIV	1.32 ± 0.13	−1.18 ± 0.13	0.71 ± 0.13	1.12 ± 0.12
KVIS	1.73 ± 0.17	−2.71 ± 0.18	0.37 ± 0.18	2.21 ± 0.17
KVSK	5.66 ± 0.30	−6.10 ± 0.28	0.63 ± 0.29	1.57 ± 0.29
LFEL	3.62 ± 0.17	−4.12 ± 0.17	0.90 ± 0.17	1.41 ± 0.17
MJSK	5.08 ± 0.23	−4.74 ± 0.24	0.48 ± 0.23	3.02 ± 0.23
MOHA	0.89 ± 0.21	−0.25 ± 0.20	1.14 ± 0.20	0.43 ± 0.20
MYVA	2.87 ± 0.19	−2.79 ± 0.18	1.25 ± 0.18	2.43 ± 0.19
NYLA	1.01 ± 0.11	−0.80 ± 0.10	0.32 ± 0.10	1.29 ± 0.10
OFEL	5.67 ± 0.34	−5.14 ± 0.33	0.04 ± 0.33	2.14 ± 0.33
OLKE	0.42 ± 0.10	−2.34 ± 0.10	0.41 ± 0.09	0.89 ± 0.10
REYK	1.84 ± 0.09	−2.30 ± 0.09	0.80 ± 0.09	1.16 ± 0.09
RFEL	3.61 ± 0.23	−3.25 ± 0.22	0.24 ± 0.22	1.42 ± 0.22
RHOF	1.42 ± 0.12	−1.43 ± 0.11	0.34 ± 0.11	0.96 ± 0.12
SARP	1.68 ± 0.21	−2.36 ± 0.20	0.73 ± 0.20	1.34 ± 0.21
SAUD	5.47 ± 0.14	1.96 ± 0.14	1.19 ± 0.14	0.17 ± 0.14
SAUR	2.05 ± 0.11	−3.13 ± 0.11	0.28 ± 0.10	1.54 ± 0.11
SAVI	3.21 ± 0.17	−3.03 ± 0.18	−0.12 ± 0.18	2.16 ± 0.18
SELC	2.03 ± 0.23	−0.88 ± 0.21	0.47 ± 0.22	1.15 ± 0.20
SELF	2.65 ± 0.09	−1.80 ± 0.09	0.65 ± 0.09	1.39 ± 0.09
SIFJ	3.99 ± 0.19	−2.77 ± 0.19	0.27 ± 0.19	1.83 ± 0.19
SKDA	2.69 ± 0.17	−3.78 ± 0.17	1.27 ± 0.17	1.46 ± 0.17
SKOG	3.64 ± 0.27	−4.35 ± 0.27	0.03 ± 0.26	1.60 ± 0.27
SKRO	5.22 ± 0.13	−5.65 ± 0.12	0.23 ± 0.12	1.36 ± 0.13
STKA	5.23 ± 0.13	−4.50 ± 0.13	0.84 ± 0.13	1.41 ± 0.13
STOR	2.55 ± 0.10	−2.56 ± 0.10	0.52 ± 0.10	1.50 ± 0.10
THEY	3.04 ± 0.15	−2.94 ± 0.15	0.34 ± 0.15	1.16 ± 0.15
THRC	2.52 ± 0.26	−3.77 ± 0.26	1.45 ± 0.25	2.57 ± 0.26
VMEY	1.50 ± 0.08	−1.94 ± 0.08	0.08 ± 0.08	1.13 ± 0.08
VOGS	0.98 ± 0.09	−1.32 ± 0.09	0.44 ± 0.09	1.24 ± 0.09

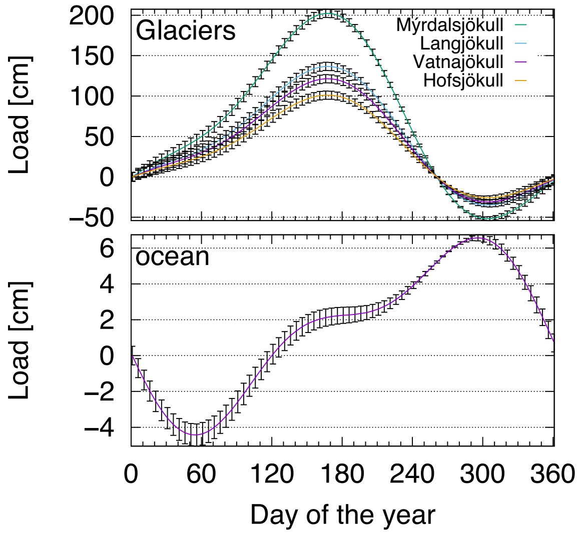

Figure A1. Seasonal cycle for glaciers and ocean loads obtained from inverting the cGPS vertical seasonal cycles using the PREM Green's function scaled by 2.3. Glaciers loads were inverted as a unique load in which each glacier load was scaled according to the ratio of their *a priori* relative mass balances (see the text). Effects from atmosphere and snow load in non-glaciated areas are removed before the inversion and stations close to Hálslón are not included. Load is given in centimetres of water equivalent. Seasonal cycle is relative to January 1. Error bars show $1-\sigma$ standard deviation.

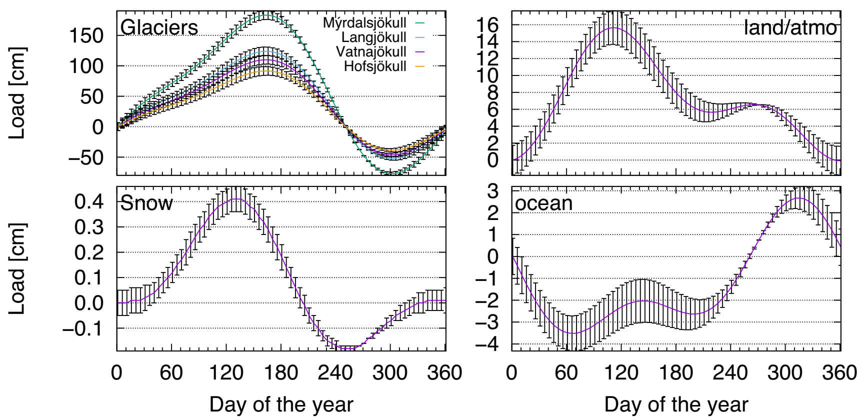

Figure A2. Seasonal cycle for glaciers, atmosphere, ocean and snow loads obtained from inverting the cGPS vertical seasonal cycles using the PREM Green's function scaled by 2.3. Glaciers loads were inverted as a unique load in which each glacier load was scaled according to the ratio of their *a priori* relative mass balances (see the text). Snow load is given as a fraction of the *a priori* snow load on day 91 (see the text). Stations close to Hálslón are not included in the inversion. Load is given in centimetres of water equivalent. Seasonal cycle is relative to January 1. Error bars show $1-\sigma$ standard deviation.

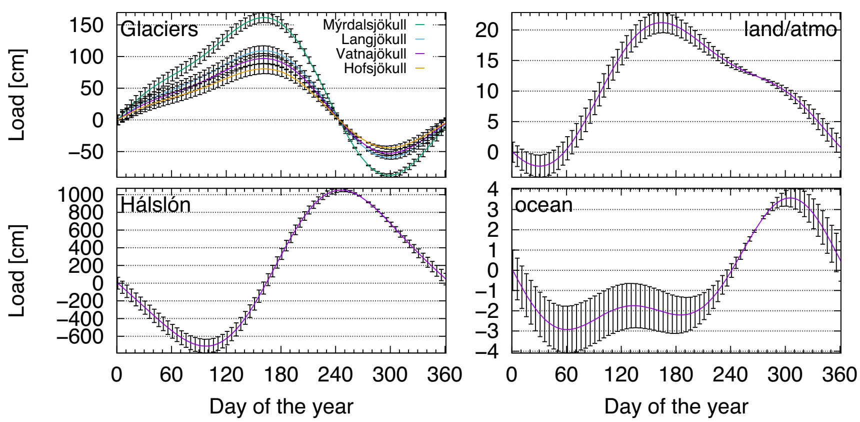

Figure A3. Seasonal cycle for glaciers, atmosphere, ocean and Hálslón loads obtained from inverting the cGPS vertical seasonal cycles using the PREM Green's function scaled by 2.3. Glaciers loads were inverted as a unique load in which each glacier load was scaled according to the ratio of their *a priori* relative mass balances (see the text). Effects from snow load in non-glaciated areas are removed before the inversion. Load is given in centimetres of water equivalent. Seasonal cycle is relative to January 1. Error bars show $1-\sigma$ standard deviation.

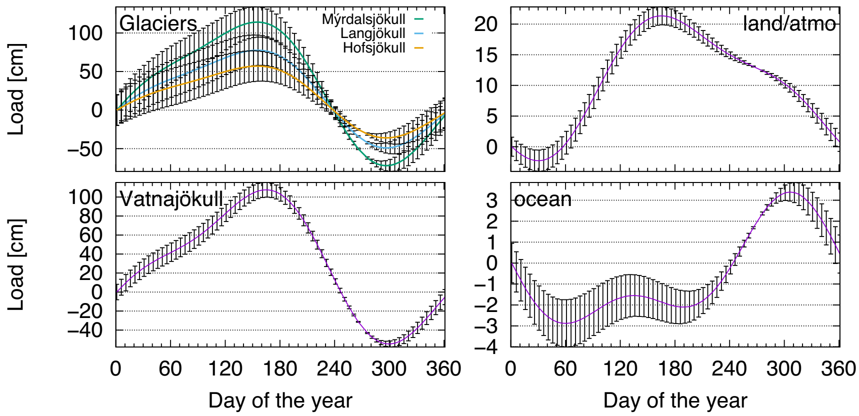

Figure A4. Seasonal cycle for glaciers, atmosphere, ocean and Hálslón loads obtained from inverting the cGPS vertical seasonal cycles using the PREM Green's function scaled by 2.3. Vatnajökull is independent while Mýrdalsjökull, Langjökull and Hofsjökull loads were inverted as a unique load in which each glacier load was scaled according to the ratio of their *a priori* relative mass balances (see the text). Effects from snow load in non-glaciated areas are removed before the inversion and stations close to Hálslón are not included. Load is given in centimetres of water equivalent. Seasonal cycle is relative to January 1. Error bars show $1-\sigma$ standard deviation.

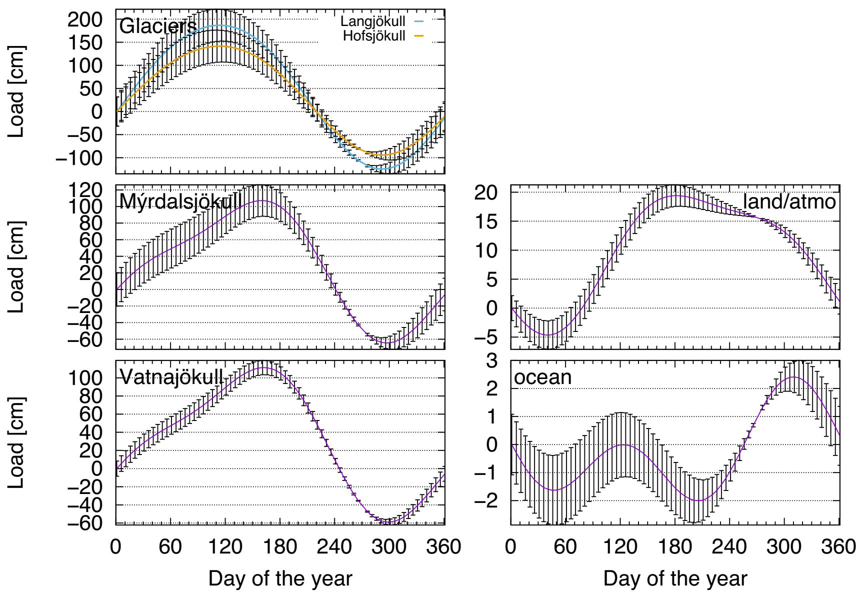

Figure A5. Seasonal cycle for glaciers, atmosphere, ocean and Hálslón loads obtained from inverting the cGPS vertical seasonal cycles using the PREM Green's function scaled by 2.3. Vatnajökull and Mýrdalsjökull are independent while Langjökull and Hofsjökull loads were inverted as a unique load in which each glacier load was scaled according to the ratio of their *a priori* mass balances (see the text). Effects from snow load in non-glaciated areas are removed before inversion and stations close to Hálslón are not included. Load is given in centimetres of water equivalent. Seasonal cycle is relative to January 1. Error bars show $1-\sigma$ standard deviation.